Na-Ion Intercalation and Charge Storage Mechanism in 2D Vanadium Carbide

Seong-Min Bak, Ruimin Qiao, Wanli Yang, Sungsik Lee, Xiqian Yu, Babak Anasori, Hungsui Lee, Yury Gogotsi,* and Xiao-Qing Yang**

2D vanadium carbide MXene containing surface functional groups (denoted as V_2CT_x, where T_x are surface functional groups) is synthesized and studied as anode material for Na-ion batteries. V_2CT_x anode exhibits reversible charge storage with good cycling stability and high rate capability through electrochemical test. The charge storage mechanism of V_2CT_x material during Na^+ intercalation/deintercalation and the redox reaction of vanadium are studied using a combination of synchrotron based X-ray diffraction, hard X-ray absorption near edge spectroscopy (XANES), and soft X-ray absorption spectroscopy (sXAS). Experimental evidence of a major contribution of redox reaction of vanadium to the charge storage and the reversible capacity of V_2CT_x during sodiation/desodiation process are provided through V *K*-edge XANES and V $L_{2,3}$-edge sXAS results. A correlation between the CO_3^{2-} content and the Na^+ intercalation/deintercalation states in the V_2CT_x electrode observed from C and O *K*-edge in sXAS results implies that some additional charge storage reactions may take place between the Na^+-intercalated V_2CT_x and the carbonate-based nonaqueous electrolyte. The results of this study provide valuable information for the further studies on V_2CT_x as anode material for Na-ion batteries and capacitors.

1. Introduction

Na-ion batteries (NIBs) have been considered promising for large-scale energy storage applications due to their potentially low-cost and natural abundance.[1] They also may provide a viable attraction in portable storage due to elimination of need for heavy and fairly expensive copper current collectors. Moreover, the accumulated knowledge and technology of lithium-ion batteries (LIBs) enables fast advancements of NIBs research since the operating principles of the NIBs are similar to that of "rocking-chair" mechanism in LIBs.[2] Although many concepts can be adopted from LIB to NIB research, the electrochemistry of NIBs turns out to be quite different than that of LIBs in many aspects, demanding new electrode materials and electrolytes to improve the performance of NIBs. As one important difference, Na^+ has a larger ionic radius than Li^+, which directly affects the mass transport and storage in the electrochemical reactions. This problem makes the currently used LIB anode materials, such as graphite, unsuitable for NIBs.[1a,3] Therefore, it is critical to develop new suitable anode materials for NIBs and carry out fundamental studies on their charge storage mechanisms.

Large class of 2D transition metal carbides and nitrides, so-called MXenes, is receiving more and more attention.[4] MXenes have shown promising potential in electrochemical energy storage applications due to their high electrical conductivity, good structural/chemical stability, and large redox-active surface areas.[4] It is predicted that MXenes can accommodate cations larger than Li^+ such as Na^+ and K^+, because of the laminar nature of MXenes with their layers bonded by weak van der Walls forces and the inherent larger interlayer spacing.[5] Indeed, several theoretical calculation studies have predicted that even two layers of Na^+ ions can be intercalated between MXene layers[6] which is confirmed by a transmission electron microscopy study.[7] However,

Dr. S.-M. Bak, Dr. H. Lee, Dr. X.-Q. Yang
Chemistry Division
Brookhaven National Laboratory
Upton, NY 11973, USA
E-mail: xyang@bnl.gov

Dr. R. Qiao, Dr. W. Yang
Advanced Light Source
Lawrence Berkeley National Laboratory
Berkeley, CA 94720, USA

Dr. S. Lee
X-Ray Science Division
Argonne National Laboratory
Argonne IL 60439, USA

Prof. X. Yu
Institute of Physics
Chinese Academy of Science
Beijing 100190, China
E-mail: xyu@iphy.ac.cn

Prof. B. Anasori, Prof. Y. Gogotsi
Department of Material Science and Engineering
A.J. Drexel Nanomaterials Institute
Drexel University
Philadelphia, PA 19104, USA
E-mail: gogotsi@drexel.edu

DOI: 10.1002/aenm.201700959

most of the studies on their electrochemical behaviors as anode materials for NIBs have been focused on the theoretical calculations only and not many systematical experimental studies have been reported. To date, only Ti_2C[8] and Ti_3C_2[7] have been experimentally studied as anode materials for nonaqueous Na-ion capacitors and NIBs, respectively. Kajiyama et al. reported the electrochemical reaction mechanism of Ti_3C_2 based on the structural changes examined by X-ray diffraction (XRD) and solid state ^{23}Na magic angle spinning NMR analyses during Na^+ intercalation/deintercalation.[9] Their work revealed that the interlayer distance of Ti_3C_2 MXene is maintained during the whole sodiation/desodiation process due to the pillaring effect of trapped Na^+ ions and the swelling effect of penetrated solvent molecules between Ti_3C_2 MXene sheets. However, the charge storage mechanism of MXenes is not fully understood yet, mainly due to the lack of answers to the basic questions such as: where does the redox reaction take place and what elements are the major contributor to the redox process during the charge storage? Therefore, it is important to study the electronic state changes associated with redox reactions, in addition to the structural changes by XRD, for further understanding of charge storage mechanisms of MXenes in NIBs.

Among different MXenes known to date, V_2C has not received much attention in NIBs so far, although the theoretical studies predicted it might be one of the most promising anode materials for NIBs. It has already shown promise as a cathode for Na-ion capacitors.[10] From previous studies, it is known that MXenes synthesized using hydrofluoric acid (HF) contain oxygenated and fluorinated surface functional groups such as −O, −OH, and −F.[5,11] Therefore, V_2C synthesized this way is denoted as V_2CT_x to indicate the presence of surface functional groups as T_x. Please note that the effects of such surface chemistry are not the subjects of this work. In this study, we report on the electrochemical properties and the charge storage mechanism of V_2C MXene as anode material for NIBs. To do so, we used XRD, hard X-ray absorption near edge spectroscopy (XANES), and soft X-ray absorption spectroscopy (sXAS) were used to study the structural, physical, and chemical properties of V_2CT_x when used as anode material for NIBs in order to understand its charge storage mechanisms. The combined use of XANES and sXAS provides very important information about the redox reaction evidenced by the electronic state changes in each element of V_2CT_x (i.e., V, C, and O).

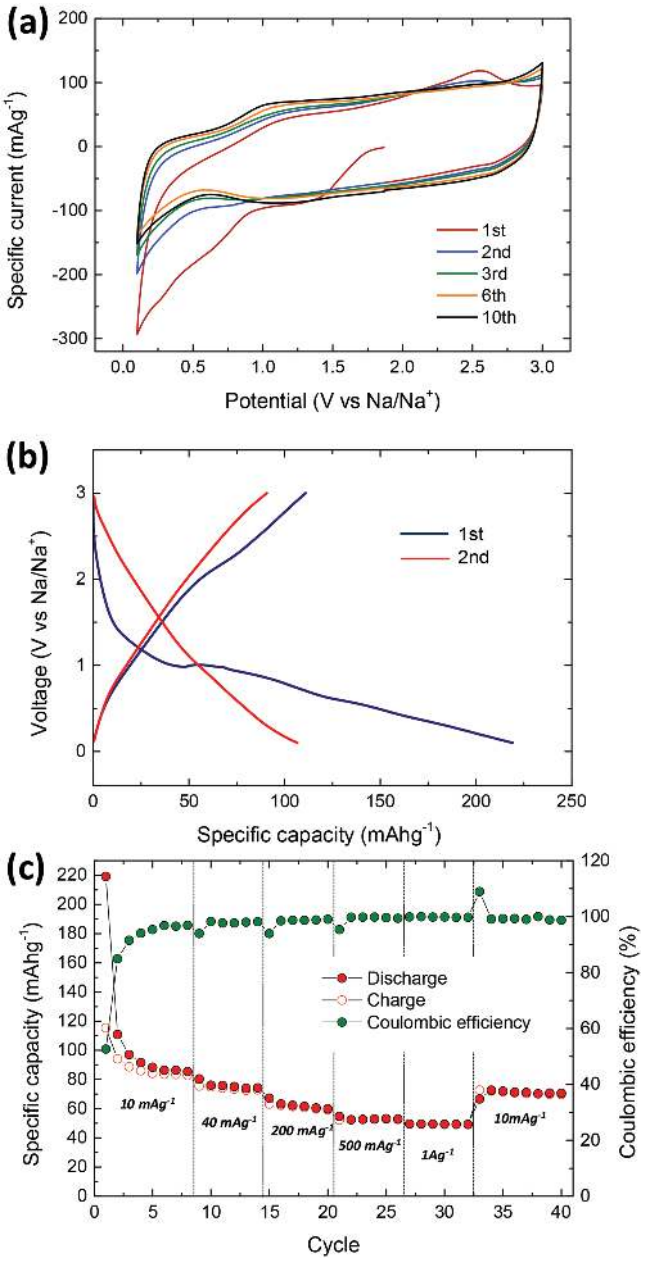

Figure 1. a) Cyclic voltammetry for V_2CT_x in a 1 M $NaPF_6$/EC–DMC electrolyte at a scan rate of 1 mV s^{-1}, b) galvanostatic charge/discharge curves measured between the cut off voltages of 0.1–3.0 V (vs Na/Na^+) at 10 mA g^{-1}, and c) change of the capacity during galvanostatic charge/discharge at different rate.

2. Results and Discussion

2.1. Electrochemical Sodium-Storage Behavior in V_2CT_x MXene

Electrochemical measurements were carried out to observe the feasibility of using V_2CT_x MXene in Na-ion batteries and capacitors. However, since the goal of this work was a fundamental study of Na-ion insertion, we did not focus on electrode optimization and maximizing electrochemical performance. **Figure 1**a shows cyclic voltammetry (CV) curves of V_2CT_x anode in a 1 M $NaPF_6$/ethylene carbonate (EC)–dimethyl carbonate (DMC) electrolyte using 1 mV s^{-1} scan rate. The first cathodic scan exhibits an irreversible current below 1.0 V (vs Na/Na^+) while all of the subsequent CV cycles exhibit the stable quasi-rectangular CVs. The lack of a strong, well-defined redox peak in the CVs of V_2CT_x corresponds to typical pseudocapacitive charge storage behavior. The large irreversible current at the first cathodic scan is most likely due to the formation of solid electrolyte interphase (SEI) layer. A similar CV behavior has been previously reported in other MXenes using both aqueous and nonaqueous electrolytes.[8,12] For example, $Ti_3C_2T_x$ cycled in aqueous electrolyte (i.e., 1 M Na_2SO_4) exhibits a quasi-rectangular CV attributed to pseudocapacitive charge storage.[12] Also, Ti_2CT_x cycled in

nonaqueous electrolyte, i.e., 1 M $NaPF_6$/EC-DEC, shows stable rectangular CVs.[8]

Figure 1b shows the galvanostatic charge/discharge curves measured in the voltage range of 0.1–3.0 V (vs Na/Na^+) at 10 mA g^{-1} in a half cell using nonaqueous electrolyte. The first discharge curve exhibits a voltage plateau at ≈1.0 V, delivering 220 mA h g^{-1} total capacity. The following first charge curve shows a capacitive slope but with a much smaller capacity of ≈125 mA h g^{-1}, resulting in a low Coulombic efficiency of 53% for the first cycle. Such large irreversibility and low Coulombic efficiency of V_2CT_x at initial few charge/discharge cycles, are similar to the previously reported results for Ti_2CT_x[8] and $Ti_3C_2T_x$.[9] The irreversible capacity loss is most likely caused by side reactions such as SEI formation and electrolyte decomposition. However, after the few initial cycles, the subsequent charge/discharge curves exhibit typical capacitor-like shape in whole voltage range, with a reversible capacity of ≈90 mA h g^{-1} at a current density of 10 mA g^{-1}. The V_2CT_x exhibits good rate capability as shown in Figure 1c. Even when cycled at very high rate of 1 Ag^{-1}, still 56% of the 90 mA h g^{-1} initial capacity at 10 mA g^{-1} can be remained. After that, when a low rate of 10 mA g^{-1} is used, a reversible capacity of 83 mA h g^{-1} can be restored. The constant current charge/discharge cycling at 20 mA g^{-1} is also shows good cycle stability with specific capacity of ≈78 mA h g^{-1} up to 100 cycles (Figure S1, Supporting Information). The good cycle stability and high rate capability of V_2CT_x make this material a potential candidate for energy storage applications, if the capacity can be significantly increased. As shown in Figure S2 (Supporting Information), some diffraction peaks representing the precursor ternary carbide residue (i.e., V_2AlC) are observed in the XRD pattern for pristine V_2CT_x. Such residue may reduce the charge/discharge capacity.[10] Also, design of the electrode architecture is of the extreme importance for achieving high capacity.[13] In addition, it is believed that the irreversible capacity loss during the first cycle can be reduced in the future by optimizing the composition of the electrolytes as well as using advanced additives. Therefore, the capacity of this material can be further improved, by optimizing the synthesis method and improving quality of MXene[14] as well as choosing suitable electrolyte.

2.2. Charge Storage Mechanism in V_2CT_x MXene

2.2.1. X-Ray Diffraction

Based on the lamellar structure of V_2CT_x, its charge storage mechanism is closely related to the Na^+ ion intercalation/deintercalation between V_2CT_x layers. Synchrotron-based ex situ and in situ XRD experiments were carried out to monitor the bulk structural changes upon Na^+ ion intercalation/deintercalation during electrochemical cycling.

Figure 2a presents ex situ XRD patterns at the 2θ angle range corresponding the (002) reflection of V_2CT_x at several

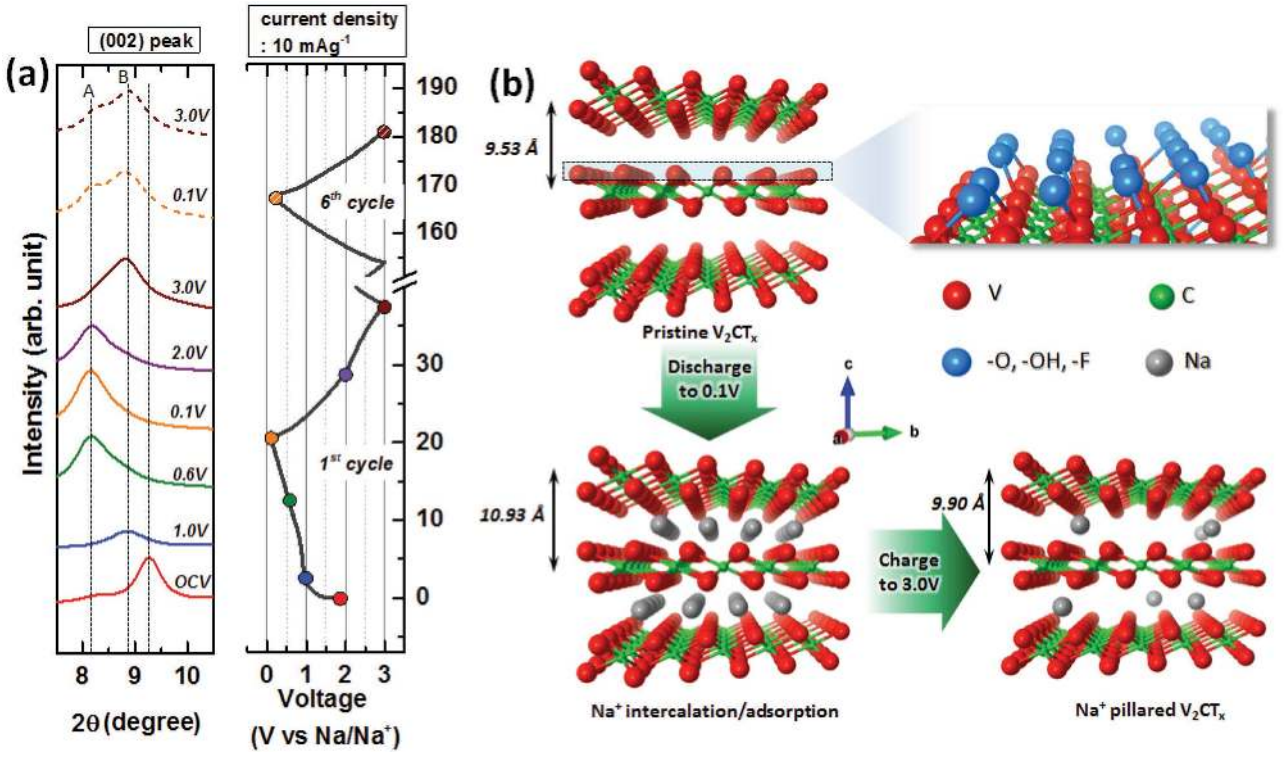

Figure 2. a) Ex situ XRD patterns (left) for V_2CT_x upon electrochemical sodiation/desodiation cycling (right). The (002) peak shifts during the first charge/discharge represent the change in the V_2CT_x interlayer spacing. The (002) peaks for the sixth cycle are shown at the top by dashed lines. b) Schematic illustration of the expansion/contraction behavior of V_2CT_x during sodiation/desodiation: the interlayer distance of V_2CT_x is increased upon Na^+ intercalation during sodiation process, then partially reduced upon Na^+ deintercalation, because of the trapped Na^+ between V_2CT_x layers, which behaves as a pillar during desodiation.

charge/discharge (i.e., sodiation/desodiation) states during the first cycle. The charge–discharge curve is also plotted on the right panel of Figure 2a. During the first sodiation process, the (002) diffraction peak in the XRD pattern moved from 9.3° to 8.1° from the open circuit voltage (OCV) state to the 0.1 V state, corresponding to an expansion of *c*-lattice parameter (*c*-LP) of V_2CT_x from 19.0 to 21.8 Å. As illustrated in Figure 2b, beside the Na^+ adsorption at the surface of V_2CT_x, that resulted in the double-layer storage, additional energy storage also occurred through Na^+ intercalation between the layers of V_2CT_x. This behavior is similar to that of previously reported Ti_2CT_x and V_2CT_x MXene materials.[8,11] However, during subsequent desodiation (or deintercalation) process, the contraction of interlayer distance (≈1.03 Å) is much smaller than the 1.40 Å expansion during the first sodiation. In situ XRD during first sodiation/desodiation was also carried out, in order to confirm the expansion/contraction behavior of V_2CT_x. The expansion/contraction of *c*-LP from in situ XRD data (plotted in Figure S3 in the Supporting Information) is consistent with ex situ XRD results. Such irreversible expansion/contraction during Na^+ intercalation/deintercalation had been reported for other MXene materials, such as Ti_2CT_x[8] and $Ti_3C_2T_x$.[10] Wang et al. reported that the interlayer distance of Ti_2CT_x increases from 7.7 to 10.1 Å during the initial sodiation but no more changes of this distance are observed during subsequent sodiation/desodiation.[8] This irreversible behavior implies that some residual Na^+ ions may not be fully deintercalated during desodiation and remain as pillars between the V_2CT_x layers. The XRD patterns for the V_2CT_x electrodes after six cycles shown in the top part of Figure 2a provides further support of this hypothesis. Interestingly, two peaks (marked as peaks A and B shown with dashed lines) are observed in the (002) peak region for the sample after six cycles of charge/discharge. The two XRD patterns for fully sodiated (0.1 V) and fully desodiated (3.0 V) samples after six cycles are quite similar, except the intensity ratio of A to B peak is larger at the 0.1 V state. The peak A appears at the same position as the peak for the first fully discharged sample, while the peak B is at the same position for the first fully charged sample. This double peak feature of the (002) reflection indicates the coexistence of two different interlayer spacings and implying the Na^+ ion were trapped in the V_2CT_x structure.

The origin of this Na^+ trapping in the V_2CT_x structure is not fully understood yet. According to Wang et al.[8] and Kajiyama et al.[9] studies on $Ti_3C_2T_x$ MXene, it might be related to the interaction between Na^+ ions and the surface functional groups of MXene layers, as well as the formation of a stable SEI.[8,10] Kajiyama et al.[9] also proposed that both, the trapped Na^+ and a stable SEI layer, are responsible for keeping the interlayer distance constant during the sodiation/desodiation and lead to high cycle stability of Ti_3CT_x electrode.[9]

2.2.2. Hard XANES

In order to study the oxidation state change of vanadium during the sodiation/desodiation, hard XANES spectra for V_2CT_x at several different discharge–charge voltages were measured. XANES, as a powerful tool to probe the oxidation states of elements, has been successfully used in the past to study the charge storage mechanism.[12,15] The ex situ V *K*-edge XANES spectra presented in **Figure 3**a were measured on samples harvested from cells discharged and charged to different voltages during the first cycle (OCV→0.1 V→3 V), as shown on the charge/discharge curve in Figure 3b.

The V *K*-edge XANES spectra presented in Figure 3a show a relatively weak pre-edge peak (marked as A) at 5470 eV

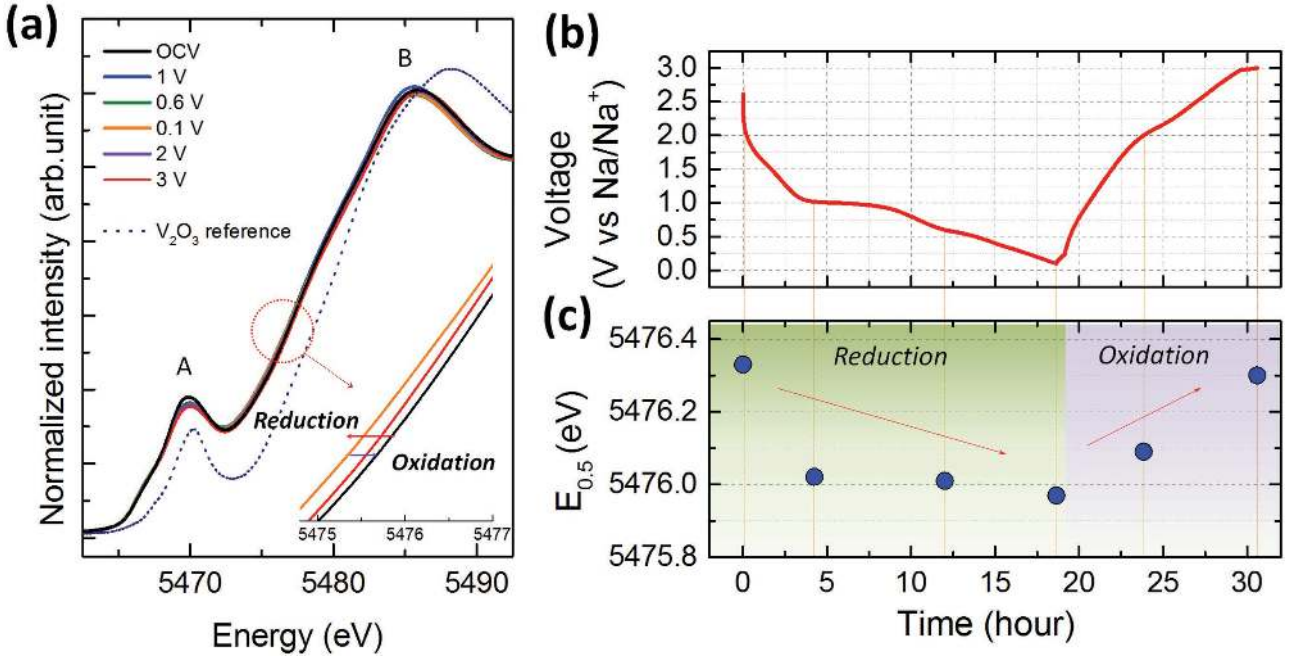

Figure 3. a) Ex situ V *K*-edge XANES spectra of V_2CT_x at selected cell voltages during first sodiation/desodiation process (OCV→0.1 V→3 V), b) corresponding voltage profile, and c) variation of V edge energy (at half height of normalized XANES spectra) at selected cell voltage.

and a strong main absorption peak (marked as B) at around 5485 eV. The pre-edge absorption is associated with the transition to hybridized electronic states of the metal 3d and carbon 2p orbitals.[16] The pre-edge peak of V_2CT_x spectra can be assigned to the transition of a 1s electron to the hybridized t_{2g} (V 3d + C 2p) and e_g (V 3d + C 2p) orbitals. And the main absorption peak "B" involves the dipole allowed transition of 1s electrons to unoccupied V 4p states.

The spectra for V_2CT_x at different discharge/charge states do not show significant differences in shapes, but the edge shift is clearly observable during both discharge and charge process (inset in Figure 3a). A plot of the V *K*-edge energies, at half height of normalized XANES spectra, as a function of sodiation/desodiation state in Figure 3c clearly show the consistent energy position changes from one voltage step to the next. During first sodiation process from OCV to 0.1 V, the edge shifts to lower energy, which reflects the reduction of vanadium. During desodiation process from 0.1 to 3 V, the edge shifts back to the higher energy indicating the oxidation of vanadium. In order to confirm these changes, in situ XAS were measured during the first cycle. The results plotted in Figure S4 (Supporting Information) show systematic edge shift upon sodiation/desodiation consistent with the ex situ results. The corresponding edge-shift (i.e., oxidation state changes of vanadium) is less irreversible in contrast to the large irreversible capacity loss observed at the first sodiation process. These results provide experimental evidence of reversible oxidation state changes at transition metal (M) in MXene relating to the electrochemical sodiation/desodiation process, with the important implication about the major contribution to charge storage of MXenes in NIB might be coming from the redox reaction at the metal elements, in our case the vanadium.

In order to verify this hypothesis, we tried to quantified the oxidation state changes of vanadium by comparing the average oxidation state and half height intensity of edge energy of V *K*-edge XANES spectra for V_2CT_x with the reference vanadium oxides (i.e., V_2O_5, VO_2, and V_2O_3), as shown in **Figure 4**. Based on the linear relationship between the edge energy and average oxidation state,[17] the oxidation state of vanadium can be roughly estimated in the V_2CT_x electrode at each voltage step. In order to avoid the uncertainties introduced by other side reactions during the first sodiation process, we only used the data from the first desodiation process.

During the first desodiation, the average oxidation state change of vanadium is about the charge of 0.2 electron (i.e., by ≈0.2 $\bar{e}$ per V atom) over the voltage range from 0.1 to 3 V. To check the viability of this value, the corresponding capacity was estimated by using the following formula: $C_g = F\delta/M_w$, where C_g [mA h g^{-1}] stands for gravimetric capacity, F [96485 C mol^{-1}] is Faraday's constant, δ is number of electrons participating in electrochemical reaction (equal to 0.2 × 2 = 0.4 in this study since there are two V atoms in V_2CT_x), M_w [g mol^{-1}] is the molar weight, and the assumed electrochemical reaction is

$$V_2CT_x + \delta\bar{e} + \delta Na^+ \rightarrow Na_\delta V_2CT_x \quad (1)$$

The overall formula weight of V_2CT_x is assumed as 114 g mol^{-1} based on the nominal molar weight for V_2C. The specific capacity value of 94 mA h g^{-1} was obtained.

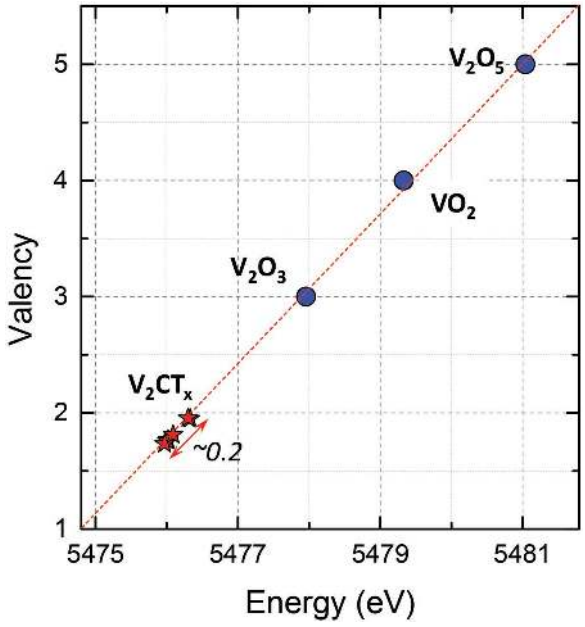

Figure 4. Average vanadium oxidation state determination in V_2CT_x during sodiation/desodiation process, using the V *K*-edge energy shift of the reference V_2O_3, VO_2, and V_2O_5 compounds.

Considering that the real formula weight of V_2CT_x is heavier than the bare V_2C (due to the presence of the T_x functional groups), the true specific capacity value should be smaller than 94 mA h g^{-1}. This estimated value is in a good agreement with the experimental capacity of 90 mA h g^{-1} obtained for the first desodiation step, although this method is semiempirical and the estimation is rather rough. It is worthwhile to note that the reversible redox behavior of V was observed from the edge-shift of ex situ XAS spectra for cycled V_2CT_x (at sixth cycle) samples (spectra are shown in Figure S5 in the Supporting Information).

These results are quite important in showing that the electrochemical redox reaction mainly takes place at the vanadium sites during sodiation/desodiation process, and this redox reaction is the major contributor to the reversible capacity of V_2CT_x. In addition, they also provide evidence supporting the statement made earlier in this paper about the irreversible capacity loss being mainly caused by the irreversible side reactions, such as SEI formation and/or electrolyte decomposition during first sodiation process.

2.2.3. Soft X-Ray Absorption Spectroscopy

Although the V *K*-edge XANES results plotted in Figures 3 and 4 show clear evidence of the contribution of Vanadium oxidation state changes to the charge storage, it would be more convincing if a direct probe of V 3d state changing during sodiation could be performed. Soft X-ray absorption spectroscopy is a more direct probe of the transition metal 3d oxidation states and chemical bonds through the diploe allowed 2p–3d transitions.[18] Therefore, the sXAS of the V $L_{2,3}$-edge on a series of V_2CT_x electrodes with different charge/discharge states were carried out to reveal directly the evolution of the vanadium

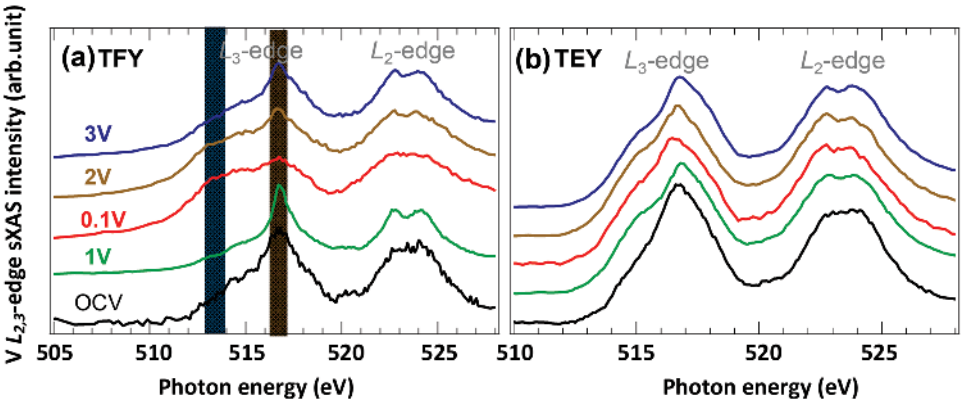

Figure 5. V $L_{2,3}$-edge sXAS spectra collected on electrodes that were cycled to different voltages. a) Bulk-sensitive total fluorescence yield (TFY) and b) surface-sensitive total electron yield (TEY).

unoccupied 3d states. In addition, the two typical detection modes of sXAS were used: the total electron yield (TEY) with a probe depth of about 10 nm; and the total fluorescence yield (TFY) with a probe depth of about 100 nm depending on photon energies; providing the information about the differences between the surface and the bulk of a battery electrode.[19] We also collected the C and O *K*-edge sXAS spectra in both TEY and TFY modes on a series of V_2CT_x electrodes to reveal the surface chemistry evolution of V_2CT_x upon electrochemical cycling.

Figure 5 shows the V $L_{2,3}$-edge sXAS spectra collected from five V_2CT_x electrodes cycled to different voltages using both (a) bulk-sensitive TFY and (b) surface-sensitive TEY. The overall sXAS spectra can be divided into two regions, the L_3-edge at the energy range of 510–520 eV and the L_2-edge at 520–530 eV, originated from the 2p core hole spin-orbital splitting. The L_2-edge displays much broader features than the L_3-edge due to shorter lifetime of the $2p_{1/2}$ core holes and the near-threshold Coster–Kronig decay.[20] Therefore, we focus on the line shape of the V L_3-edge in this work. It is apparent that L_3-edge in TFY spectra display dramatic voltage-dependent changes, which are related to the vanadium redox reactions in the bulk V_2CT_x. The 516.7 eV peak intensity decreases from 1–0.1 V and increases from 0.1 to 3 V, while the lower energy peak at 513 eV shows just the opposite trend. The two sXAS features are related to the two different oxidation states of V, i.e., the high energy peak at 516.7 eV represents a higher oxidation state and its intensity increases when the average oxidation state of vanadium increases.[21] Therefore, the changes in sXAS intensity and line shape changes clearly demonstrate the reduction of the V ions during the initial discharge from 1.0 down to 0.1 V. Unlike in the V *K*-edge spectra, where the reduction of average oxidation of vanadium was indicated by the edge shift to lower energy, for the L_3 edge spectra, such reduction is indicated by the reduction of intensity ratio of 516.7 eV/513 eV peaks, which can be clearly observed by the significant enhancement of the 513 eV peak intensity at 0.1 V (sodiated).[21]

Due to the sensitivity of the transition-metal *L*-edge sXAS to the valence 3d,[18] the data in Figure 5 also show clearly that the V *L*-edge line shape does not fully recover when the V_2CT_x electrode is charged back to 3 V from its discharged state (0.1 V). This indicates that the V redox is not fully reversible in the initial cycle, which is consistent with the low Coulombic efficiency obtained by electrochemical test. Another observation is that the surface-sensitive TEY spectra (Figure 5b) show much weaker change, compared with that of the bulk-probing TFY (Figure 5a), indicating less changes in vanadium oxidation states at the surface of V_2CT_x electrode during cycling. Combining these results with those of XRD and V *K*-edge XANES, it can be concluded that the redox reaction of vanadium mainly takes place in the bulk of V_2CT_x during Na^+ intercalation/deintercalation rather than at the surface. Thus, the entire volume of the MXene particles is intercalated by Na ions and most of the charge has been stored due to intercalation, rather than a double layer on the externally accessible surfaces.

Another critical issue associate with anode materials is the surface reactions during the electrochemical cycling. The voltage dependent sXAS studies of the surface C and O species of the V_2CT_x electrodes were also carried out. The results are shown in **Figure 6** for C *K*-edge and **Figure 7** for O *K*-edge using both bulk-sensitive TFY and surface-sensitive TEY detections. Both the C *K*-edge and the O *K*-edge results show very interesting sodiation/desodiation state dependent evolution of the spectra during the electrochemical cycling. The three major absorption peaks on the C *K*-edge sXAS spectra are marked in Figure 6, assigned to C=C, C−H, and CO_3^{2-}, respectively.[22] The most notable change is the increased intensity of the peak representing CO_3^{2-} with increasing sodiation states of the V_2CT_x, and decreased intensity with increasing desodiation state. The same phenomena could be observed on the O *K*-edge sXAS as shown in Figure 7 the fingerprint peak of CO_3^{2-} in O *K*-edge spectra[23] evolves in the same way as in the C *K*-edge. In contrast to the V-*L* sXAS line shape evolution that manifests strongly in the bulk-sensitive TFY mode (Figure 5a), the line shape changes of the C-*K* (Figure 6) and the O-*K* spectra (Figure 7) is more pronounced in the surface-sensitive TEY mode. This suggests that the changes of the CO_3^{2-} species, unlike changes in V oxidation state, are mainly taken place at the surface. It is speculated that the reaction is occurred between the Na^+-intercalated V_2CT_x and the carbonate-based nonaqueous electrolyte solvents, i.e., EC and DMC, used in this study. However, a detailed interpretation of such changes of the sXAS spectra of the surface CO_3^{2-} species is complicated and several points may be worthwhile to mention: (1) Although

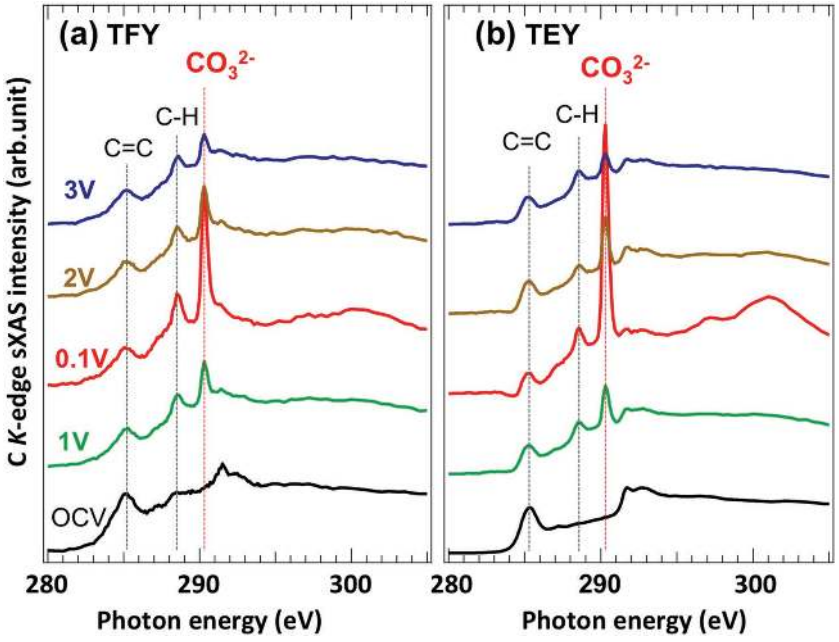

Figure 6. C *K*-edge sXAS spectra collected on electrodes that were cycled to different voltages. a) Bulk-sensitive TFY and b) surface-sensitive TEY. Vertical lines are guide to eyes of the fingerprinting features of the different chemical bonds.

the change of the CO_3^{2-} content mostly occurs at the surface, it is also observable in the bulk-sensitive TFY results. This bulk structural change is also observed from the intensity changes of Na_2CO_3 related peaks from the XRD results, as shown in Figure S6 (Supporting Information). This Na_2CO_3 related structural changes are also observed for cycled samples (Figure S7, Supporting Information), which reflect the reversibility of the reaction. Kajiyama et al. reported that the $Ti_3C_2T_x$ electrode exhibits desolvated Na^+ intercalation between the $Ti_3C_2T_x$ layers which are swelled by solvent molecule penetration.[9] Taking into account their result with our XRD data (Figure 2a), it is expected that the CO_3^{2-} content in bulk structure is not influenced by Na^+ intercalation/deintercaltion, because the solvent molecule penetration occurs only at the first sodiation process with desolvated Na^+ intercalation. Therefore, the change of CO_3^{2-} content in TFY result is not a result from the solvent intercalation/deintercalation into the V_2CT_x bulk structure. Rather than that, it is possible that a reaction take place between Na^+-intercalated V_2CT_x and the electrolyte, because the sodium-intercalated V_2CT_x is highly active. (2) Also, we note that the evolution of carbonate signal in our sXAS result indicates the instability of SEI on the electrode surface upon electrochemical cycling. (3) It is quite interesting to see the highly reversible CO_3^{2-} related reaction in this system through the C *K*-edge and O *K*-edge sXAS spectra, which is worth of further investigation, considering its potential application in Na—CO_2 battery systems, as previously reported by Hu et al.[24] (4) Finally, the possibility of CO_3^{2-} contamination of the V_2CT_x samples used in this study cannot be completely ruled out. Although the experimental process was well-controlled under zero air exposure conditions, some trace amount of H_2O, O_2, and CO_2 could be introduced even in high-purity Ar glove box.

Clarifying the detailed reaction mechanisms at the electrode–electrolyte interface has been one of the grand challenges in the battery field. The surface evolution of MXene electrodes revealed through our sXAS data justifies more detailed studies of the process. Our preliminary results on the surface CO_3^{2-} activity described in this paper provide valuable information for further studies on CO_3^{2-} related systems.

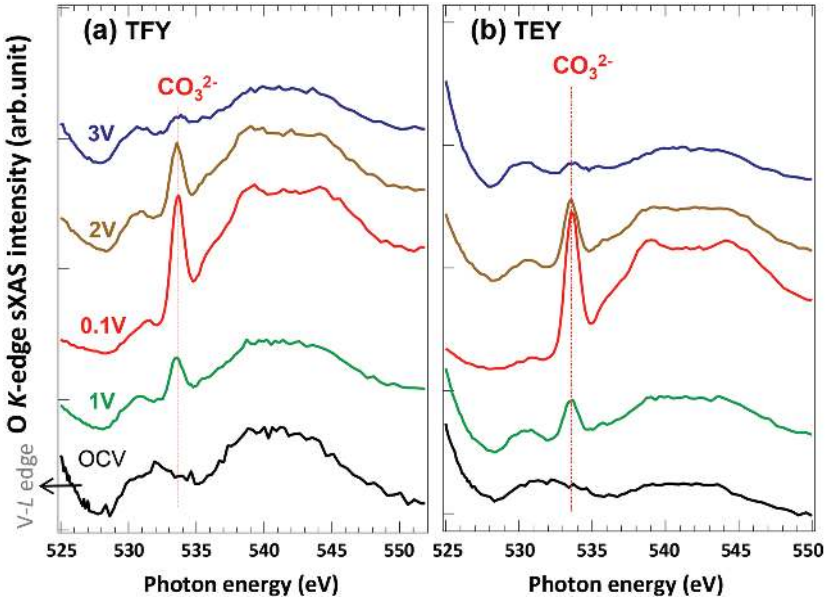

Figure 7. O *K*-edge sXAS spectra collected on electrodes that were cycled to different voltages. a) Bulk-sensitive TFY and b) surface-sensitive TEY. Vertical lines indicate the feature that corresponding to the π^* peak of the $-CO_3^{2-}$ groups.

3. Conclusion

V_2CT_x MXene shows reversible electrochemical charge storage with good cycling stability and high rate capability which are important characteristics for the high power battery and Na-ion capacitor applications. The charge storage mechanisms were studied using a combination of ex/in situ synchrotron based XRD, XANES, and sXAS. The XRD results confirm that the expansion/contraction of the interlayer space of V_2CT_x upon Na^+ intercalation/deintercalation during the first cycle. V *K*-edge XANES results clearly show the redox reaction of vanadium during the Na^+ intercalation/deintercalation, which

implies that the redox reaction at the transition metal (M) site in MXene is responsible for the electrochemical charge storage. The results of V $L_{2,3}$-edge sXAS experiments provided further direct evidence of such a redox reaction of vanadium within the MXene. In addition, C and O *K*-edge sXAS results shows potentially important features related to the reversible formation/decomposition of CO_3^{2-} species upon sodiation/desodiation. This surface related reaction is still not fully understood, but may provide valuable information for further understanding of V_2CT_x electrodes as well as CO_3^{2-} related redox systems.

4. Experimental Section

Material Synthesis and Electrochemical Test: V_2CT_x was synthesized by selectively etching the atomic layers of aluminum from V_2AlC MAX phase with a 50% concentrated HF solution for 8 h at 55 °C followed by washing the powder to raise the acidic pH to ≈6. More experimental details of material synthesis are described in the previous publication.[7,10] The electrode was fabricated by slurry coating of a mixture of active material (V_2CT_x): acetylene black: polyvinylidene fluoride binder in 8:1:1 weight ratio, onto Al foil. The electrode was dried at 80 °C in vacuum for overnight before use. A two-electrode 2032 coin cells were assembled with pure sodium metal as the counter electrode and a glass fiber as the separator in an argon-filled glove box. The electrolyte was 1 M NaPF6 dissolved in EC–DMC with the ratio of 3:7 by volume. SP-300 Potentiostat/galvanostat (Biologic SA, France) was used for electrochemical testing by cyclic voltammetry and glavanostatic charge–discharge. For the in situ XAS and XRD measurement during electrochemical testing, a two-electrode 2032 coin-type cell with two 3 mm diameter coaxial holes on both sides was used. The holes were sealed with polyimide (Kapton) tape.

Ex/In Situ XRD Measurement: Ex situ XRD data were collected at XPD-1 (28-ID-1) beamline of National Synchrotron Light Source II (NSLS-II) using 2D image plate detector. The beam was calibrated to a wavelength of 0.185794 Å, and the 2D data were integrated to simulate a 1D pattern using the Fit2D software.[25] In situ XRD measurements were performed at the beamline 17-BM-B at the Advanced Photon Source (APS) of Argonne National Laboratory (ANL), using X-rays of wavelength $\lambda = 0.72768$ Å with a Perkin-Elmer 2D plate detector in 1 min interval. A $Na_2Ca_3Al_2F_{14}$ standard was used to calibrate the sample-to-detector distance (i.e., 385.4 mm), and then the 2D diffraction patterns were radially integrated and converted to intensity versus 2θ format using the GSAS-II software.[26] For convenience, the 2θ values shown in this paper were converted to those corresponding to common laboratory Cu Kα radiation ($\lambda = 1.5406$ Å).

Ex/In Situ V K-Edge XANES Measurement: Ex situ V *K*-edge XAS measurement were performed at the beamline 12-BM at the APS and ISS beamline (8-ID) at the NSLS-II. In situ V *K*-edge XAS measurement were performed at the beamline 9-BM at the APS. All spectra were collected in transmission mode. The beam intensity was detuned to 50% of its initial intensity to minimize the high-order harmonics. Reference spectra of vanadium metallic foil was collected simultaneously with all of the spectra for energy calibration. XANES spectra were processed using the ATHENA software package.[27] The photoelectron energy origin E0 was chosen at the half height of the normalized absorption edge jump.

Ex/In Situ sXAS Measurement: V $L_{2,3}$-edge, C, and O *K*-edge sXAS measurements were performed in iRIXS endstation at beamline 8.0.1 of the advanced Light Source (ALS) at Lawrence Berkeley National Lab.[28] The undulator and spherical grating monochromator supply a linearly polarized photon beam with resolving power up to 6000. The experimental energy resolution is about 0.15 eV. Experiments were performed at room temperature and with the linear polarization of the incident beam oriented at 45° to the sample surfaces. All the spectra were normalized to the beam flux measured by the upstream gold mesh. For the measurement, a group of coin cells with the MXene electrodes were electrochemically cycled to different voltages. Afterward, they were disassembled carefully in Ar glove box then immediately rinsed with DMC to lock their electrochemical states. The electrodes were loaded into a home-designed sample transfer kit in glove box and were later directly mounted into the ultrahigh vacuum XAS characterization chamber to avoid any air exposure.

Supporting Information

Supporting Information is available from the Wiley Online Library or from the author.

Acknowledgements

S.-M.B. and R.Q. contributed equally to this work. The work done at the Brookhaven National Lab was supported by the U.S. Department of Energy, the Assistant Secretary for Energy Efficiency and Renewable Energy, Office of Vehicle Technologies, through the Advanced Battery Materials Research (BMR) Program, under Contract No. DE-SC0012704. The Advanced Light Source (ALS) was supported by the Director, Office of Science, Office of Basic Energy Sciences, of the U.S. Department of Energy under Contract No. DE-AC02-05CH11231. B.A. and Y.G. acknowledge the support of the Fluid Interface Reactions, Structures and Transport (FIRST) Center, the Energy Frontier Research Center funded by the U.S. Department of Energy, Office of Science, Basic Energy Sciences. B.A. acknowledges the help of Bernard Haines in the material synthesis process. The work at the Institute of Physics was supported by funding from the "One Hundred Talent Project" of the Chinese Academy of Sciences. The authors acknowledge technical support from the scientists at 9-BM, 12-BM, 17-BM of APS (ANL), supported by the U.S. DOE under Contract No. DE-AC02-06CH11357. The authors acknowledge technical support from the scientists at the beamlines of ISS (8-ID) and XPD (28-ID) at NSLS-II, supported by the U.S. Department of Energy, Office of Science, Office of Basic Energy Sciences, under Contract No. DE-SC0012704. The authors also acknowledge the technical support from the beamline scientists from BL2-2 of the Stanford Synchrotron Radiation Lightsource, SLAC National Accelerator Laboratory, supported by the U.S. Department of Energy, Office of Science, Office of Basic Energy Sciences under Contract No. DE-AC02-76SF00515.

Conflict of Interest

The authors declare no conflict of interest.

Keywords

charge storage, MXene, sodium-ion batteries, vanadium carbide, X-ray absorption spectroscopy

Received: April 7, 2017
Revised: May 10, 2017
Published online: July 14, 2017

[1] a) V. Palomares, P. Serras, I. Villaluenga, K. B. Hueso, J. Carretero-Gonzalez, T. Rojo, *Energy Environ. Sci.* **2012**, *5*, 5884; b) M. D. Slater, D. Kim, E. Lee, C. S. Johnson, *Adv. Funct. Mater.* **2013**, *23*, 947; c) N. Yabuuchi, M. Kajiyama, J. Iwatate, H. Nishikawa, S. Hitomi, R. Okuyama, R. Usui, Y. Yamada, S. Komaba, *Nat. Mater.* **2012**, *11*, 512.

[2] a) H. L. Pan, Y. S. Hu, L. Q. Chen, *Energy Environ. Sci.* **2013**, *6*, 2338; b) Y. S. Wang, X. Q. Yu, S. Y. Xu, J. M. Bai, R. J. Xiao, Y. S. Hu, H. Li, X. Q. Yang, L. Q. Chen, X. J. Huang, *Nat. Commun.* **2013**, *4*, 2365.
[3] S. W. Kim, D. H. Seo, X. H. Ma, G. Ceder, K. Kang, *Adv. Energy Mater.* **2012**, *2*, 710.
[4] a) M. Naguib, J. Halim, J. Lu, K. M. Cook, L. Hultman, Y. Gogotsi, M. W. Barsoum, *J. Am. Chem. Soc.* **2013**, *135*, 15966; b) Y. Xie, M. Naguib, V. N. Mochalin, M. W. Barsoum, Y. Gogotsi, X. Q. Yu, K. W. Nam, X. Q. Yang, A. I. Kolesnikov, P. R. C. Kent, *J. Am. Chem. Soc.* **2014**, *136*, 6385; c) B. Anasori, Y. Xie, M. Beidaghi, J. Lu, B. C. Hosler, L. Hultman, P. R. C. Kent, Y. Gogotsi, M. W. Barsoum, *ACS Nano* **2015**, *9*, 9507.
[5] B. Anasori, M. R. Lukatskaya, Y. Gogotsi, *Nat. Rev. Mater.* **2017**, *2*, 16098.
[6] a) C. Eames, M. S. Islam, *J. Am. Chem. Soc.* **2014**, *136*, 16270; b) E. Yang, H. Ji, J. Kim, H. Kim, Y. Jung, *Phys. Chem. Chem. Phys.* **2015**, *17*, 5000; c) Y. Xie, Y. Dall'Agnese, M. Naguib, Y. Gogotsi, M. W. Barsoum, H. L. L. Zhuang, P. R. C. Kent, *ACS Nano* **2014**, *8*, 9606.
[7] X. Wang, X. Shen, Y. Gao, Z. Wang, R. Yu, L. Chen, *J. Am. Chem. Soc.* **2015**, *137*, 2715.
[8] X. Wang, S. Kajiyama, H. Iinuma, E. Hosono, S. Oro, I. Moriguchi, M. Okubo, A. Yamada, *Nat. Commun.* **2015**, *6*, 6544.
[9] S. Kajiyama, L. Szabova, K. Sodeyama, H. Iinuma, R. Morita, K. Gotoh, Y. Tateyama, M. Okubo, A. Yamada, *ACS Nano* **2016**, *10*, 3334.
[10] Y. Dall'Agnese, P. L. Taberna, Y. Gogotsi, P. Simon, *J. Phys. Chem. Lett.* **2015**, *6*, 2305.
[11] M. Naguib, V. N. Mochalin, M. W. Barsoum, Y. Gogotsi, *Adv. Mater.* **2014**, *26*, 992.
[12] M. R. Lukatskaya, S. M. Bak, X. Q. Yu, X. Q. Yang, M. W. Barsoum, Y. Gogotsi, *Adv. Energy Mater.* **2015**, *5*, 1500589.
[13] a) C. E. Ren, M.-Q. Zhao, T. Makaryan, J. Halim, M. Boota, S. Kota, B. Anasori, M. W. Barsoum, Y. Gogotsi, *ChemElectroChem* **2016**, *3*, 689; b) X. Xie, M.-Q. Zhao, B. Anasori, K. Maleski, C. E. Ren, J. Li, B. W. Byles, E. Pomerantseva, G. Wang, Y. Gogotsi, *Nano Energy* **2016**, *26*, 513.
[14] A. Lipatov, M. Alhabeb, M. R. Lukatskaya, A. Boson, Y. Gogotsi, A. Sinitskii, *Adv. Electron. Mater.* **2016**, *2*, 1600255.
[15] K. W. Nam, M. G. Kim, K. B. Kim, *J. Phys. Chem. C* **2007**, *111*, 749.
[16] J. G. Chen, *Surf. Sci. Rep.* **1997**, *30*, 1.
[17] a) M. Croft, D. Sills, M. Greenblatt, C. Lee, S. W. Cheong, K. V. Ramanujachary, D. Tran, *Phys. Rev. B* **1997**, *55*, 8726; b) J. Wong, F. W. Lytle, R. P. Messmer, D. H. Maylotte, *Phys. Rev. B* **1984**, *30*, 5596.
[18] Q. Li, R. Qiao, L A. Wray, J. Chen, Z. Zhuo, Y. Chen, S. Yan, F. Pan, Z. Hussain, W. Yang, *J. Phys. D: Appl. Phys.* **2016**, *49*, 413003.
[19] a) W. Yang, X. Liu, R. Qiao, P. Olalde-Velasco, J. D. Spear, L. Roseguo, J. X. Pepper, Y.-d. Chuang, J. D. Denlinger, Z. Hussain, *J. Electron Spectrosc. Relat. Phenom.* **2013**, *190*, 64; b) Y. Wanli, Q. Ruimin, *Chin. Phys. B* **2016**, *25*, 017104.
[20] a) J. Zaanen, G. A. Sawatzky, *Phys. Rev. B* **1986**, *33*, 8074; b) F. M. F. Degroot, J. C. Fuggle, B. T. Thole, G. A. Sawatzky, *Phys. Rev. B* **1990**, *42*, 5459.
[21] G. Cressey, C. M. B. Henderson, G. Vanderlaan, *Phys. Chem. Miner.* **1993**, *20*, 111.
[22] a) O. Dhez, H. Ade, S. G. Urquhart, *J. Electron Spectrosc. Relat. Phenom.* **2003**, *128*, 85; b) A. Augustsson, M. Herstedt, J. H. Guo, K. Edstrom, G. V. Zhuang, P. N. Ross, J. E. Rubensson, J. Nordgren, *Phys. Chem. Chem. Phys.* **2004**, *6*, 4185; c) R. M. Qiao, I. T. Lucas, A. Karim, J. Syzdek, X. S. Liu, W. Chen, K. Persson, R. Kostecki, W. L. Yang, *Adv. Mater. Interfaces* **2014**, *1*, 1300115.
[23] R. Qiao, Y. D. Chuang, S. Yan, W. Yang, *PLoS One* **2012**, *7*, e49182.
[24] X. F. Hu, J. C. Sun, Z. F. Li, Q. Zhao, C. C. Chen, J. Chen, *Angew. Chem., Int. Ed.* **2016**, *55*, 6482.
[25] A. P. Hammersley, S. O. Svensson, M. Hanfland, A. N. Fitch, D. Hausermann, *High Pressure Res.* **1996**, *14*, 235.
[26] B. H. Toby, R. B. Von Dreele, *J. Appl. Crystallogr.* **2013**, *46*, 544.
[27] J. C. Woicik, B. Ravel, D. A. Fischer, W. J. Newburgh, *J. Synchrotron Radiat.* **2010**, *17*, 409.
[28] R. Qiao, Q. Li, Z. Zhuo, S. Scallis, O. Fuchs, M. Blum, L. Weinhardt, C. Heske, J. Pepper, M. Jones, A. Brown, A. Spucces, K. Chow, B. Smith, P.-A. Glans, Y. Chen, S. Yan, F. Pan, L. F. J. Piper, J. Denlinger, J. Guo, Z. Hussain, Y.-D. Chuang, W. Yang, *Rev. Sci. Instrum.* **2017**, *88*, 033106.

